

pubs.acs.org/JACS Article

Design of a Four-Atom Cluster Embedded in Carbon Nitride for Electrocatalytic Generation of Multi-Carbon Products

Dewei Zhang, Oleg V. Prezhdo,* and Lai Xu*



Cite This: J. Am. Chem. Soc. 2023, 145, 7030-7039



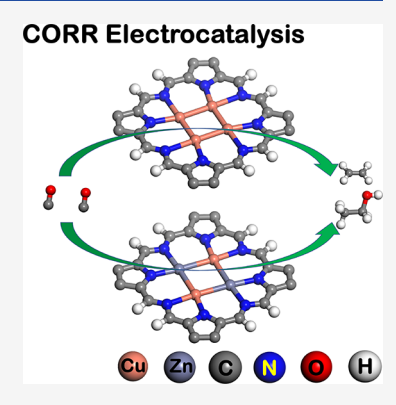
ACCESS I

III Metrics & More

Article Recommendations

Supporting Information

ABSTRACT: The development of efficient and stable catalysts for the electrocatalytic CO_2 and CO reduction reactions (CORR) is under active investigation, but the problems of poor selectivity and low efficiency for C_2 products still exist. We design a two-dimensional carbon nitride material ($C_5N_2H_2$) that contains an eight N-atom structure capable of coordinating four-metal atom clusters and supporting simultaneously two carbon oxide molecules needed for the C_2 coupling. The designed material has excellent electrical conductivity and stability. After high-throughput screening of catalytic performance of multiple four-metal clusters embedded into the framework, we systematically investigate the CORR process of 11 candidates. We find that Cu_4 - $C_5N_2H_2$ has superior selectivity and low limiting potential for generating ethylene, while Cu_2Zn_2 - $C_5N_2H_2$ is selective and efficient to synthesize ethanol. Further, we discover a novel type of descriptor related to 2D material flexibility to evaluate the potential-determining step for generating ethylene. Our report both broadens the possibilities for few-atom CO reduction and demonstrates a novel substrate flexibility-related descriptor to predict the catalytic performance of materials.



■ INTRODUCTION

Fossil fuels are still widely used as the main energy source, while clean energy such as wind energy, water energy, and solar energy are being actively developed. The fossil energy is a double-edged sword for human beings. Excessive use of energy promotes economic development and improvement of people's living standards, but it is followed by excessive emissions of greenhouse gases such as carbon dioxide. Overuse of resources has brought about an imbalance in the carbon cycle, and the sharp increase in the concentration of CO₂ has caused problems such as global warming. In recent years, some new framework materials have emerged for multiple applications; ¹⁻⁶ the electrocatalytic reduction of CO₂ or CO to more valuable hydrocarbons is considered to be an environmentally friendly and effective method and has become a significant topic in the energy field.^{7–9} It not only solves the problem of carbon imbalance but also generates high valueadded products such as C₂H₄ and C₂H₅OH, killing two birds with one stone. C_{2+} products play a vital role in current energy and chemical supplies, such as fuel additives, plastics, disinfectants, and pharmaceuticals.¹⁰ As the key intermediate of CO₂RR, the reduction conversion of CO is completely consistent with the reaction mechanism after CO adsorption in CO₂RR, and it is an ideal alternative reaction. 11-14

Therefore, it is particularly significant to find electrocatalysts with high activity, excellent stability, and eminent selectivity. Unlike other metals, Cu is the only one that can achieve multistep H transfer in the process of CO_2 or CO reduction to obtain C_{2+} products such as ethylene or ethanol. Although the Cu bulk exhibits good catalytic performance, the internal

utilization of the catalyst is not sufficient. In recent years, the emerging atomically dispersed catalysts show excellent catalytic performance due to their extremely high specific surface area and high atomic utilization. It will be of great significance to shift the focus from Cu bulk to atomic-scale Cu. Twodimensional materials have great advantages due to their multiple active sites and excellent electron transfer ability. Loading single or several atoms onto 2D nanomaterials provides a clear catalytic active center and maximizes the efficiency of atom utilization, such as single-atom catalysts, ^{15–18} dual-atom catalysts, ^{19–22} and nanocluster catalysts. ^{23–25} Previously, we designed a two-metal cluster supported 2D graphene carbon nitride catalyst for CO₂RR to achieve a lower limiting potential.¹⁹ We also designed trimetal clusters supported by C2N materials and performed high throughput screening for an efficient system for the nitrogen reduction reaction.²³ Four-atom cluster catalysts provide more active sites and a larger reaction area, which is conducive to the occurrence of C-C coupling and the generation of C2 products.

In this work, we design a 2D material for CO reduction, aiming to provide well-defined active centers for selective

Received: February 11, 2023 Published: March 15, 2023





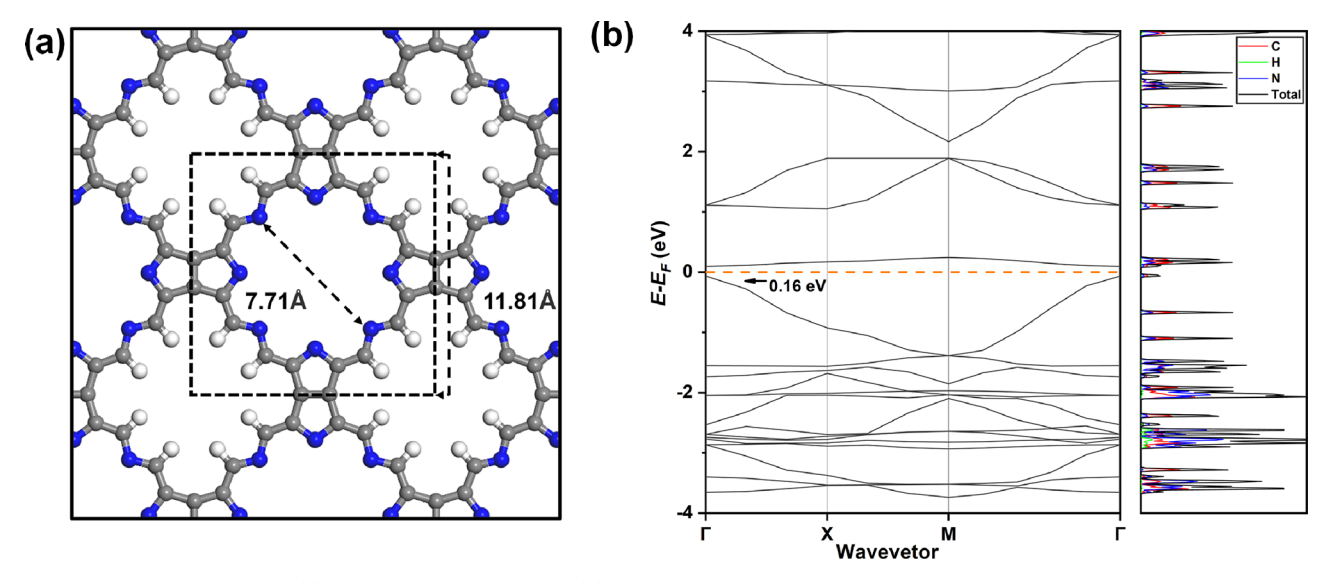


Figure 1. Optimized structures (a) and electronic properties (b) of $C_5N_2H_2$. The structural unit is marked with a dashed line. The elemental projected DOS is illustrated. The Fermi level (E_f) is set to zero.

catalysis of specific products. Through four pyrroles and four -C-N-C- linkages, a structure with eight bare N atoms was constructed, and the stability of the 2D substrate was confirmed by ab initio molecular dynamics (AIMD) and phonon spectroscopy calculations. According to the HSE06 energy band calculation, this semiconductor has a narrow band gap of only 0.16 eV with superior conductivity. Subsequently, four-metal cluster catalysts were designed based on the developed carbon nitride material, in which the eight N atomic sites can support four metal atoms. Compared with single-atom and dual-atom catalytic reactions, we propose a four-metal atom CORR catalysis mode that provides more possibilities for catalyst tuning. Involvement of multiple metals leads to synergistic effects enhancing the catalytic performance. 19,21,22,26 Tetrametal sites enable simultaneous adsorption of two CO molecules and provide the chemical environment for the subsequent coupling reaction and protonation process. In the CORR path calculation, we found that Cu_4 - $C_5N_2H_2$ has high selectivity for ethylene synthesis, with a low limiting potential of -0.50 V. Alternatively, Cu₂Zn₂-C₅N₂H₂ is an excellent catalyst to produce ethanol (-0.46 V). Further, we obtained a flexibility-related descriptor $D_{(Cu-Cu)} \times (D_{(N-N)} - 2 \times R_N)$ based on the LASSO regression. The descriptor establishes the connection between the changes in the substrate due to loading of different metals and the limiting potential for CO reduction to ethylene.

■ METHODS

Spin-polarized density functional theory (DFT) was used as implemented in the Vienna ab initio simulation package (VASP). The exchange—correlation energy was described by the Perdew—Burke—Ernzerhof (PBE) functional within the generalized gradient approximation (GGA), and the projector augmented wave (PAW) method was used to describe the electron—ion interactions. The van der Waals interaction between atoms was treated using the DFT-D3 method with Becke-Jonson damping. A 450 eV energy cutoff was adopted for the plane-wave basis. The Brillouin zone was sampled by $2\times2\times1~k$ points using the Monkhorst—Pack scheme for structural optimizations. The energy and force convergence thresholds on each atom were set to 10^{-5} eV and $0.05~eV/\mbox{Å}$, respectively. The vacuum space was fixed as 29 Å to avoid the interaction between adjacent layers.

The phonon dispersion analysis was performed for the 2×2 supercell using the Phonopy code with the density functional perturbation theory (DFPT). The ab initio molecular dynamic (AIMD) simulations were carried out to evaluate the thermodynamic stability using the NVT ensemble at 300, 500, 800, and 1000 K for 10 ps with a 1 fs time step. Solvation effects were taken into account with the VASPsol model using the dielectric constant of water at 78.5. The climbing-image nudged elastic band (CI-NEB) method was utilized to obtain the kinetic barriers. The Heyd–Scuseria–Ernzerhof (HSE06) Hybrid functional was used to compute the band structure and density of states (DOS).

To obtain the electron chemical potential by adjusting the number of charges, grand canonical DFT calculations were performed using the JDFTx³⁵ code with explicit constant electrochemical potential (μ e). The cutoff energy was set to 17 Hartree, and the CANDEL³⁶ implicit solvation model was also used. The cohesive energy (E_c) was calculated by the following equation

$$E_c = \frac{E_{\text{sub}} - \sum_i n_i E_i}{n} \tag{1}$$

where E_{sub} is the total energy of $C_5N_2H_2$ in this work, ni and E_i are the number of atoms of type i=C, N, and H in the unit cell and the corresponding energies, and n is total number of atoms. The formation energy (E_f) was defined as

$$E_f = (E_{\text{sub-m}} - E_{\text{sub}} - 4E_{\text{m}})/4 \tag{2}$$

where $E_{\text{sub}-m}$ is the total energy of M_4 - $C_5N_2H_2$, E_m is the energy of the metal atom in its most stable bulk structure, and E_{sub} is the energy of the substrate. The adsorption energies (ΔE_a) of the CO molecule and the H atom on the substrate were obtained by

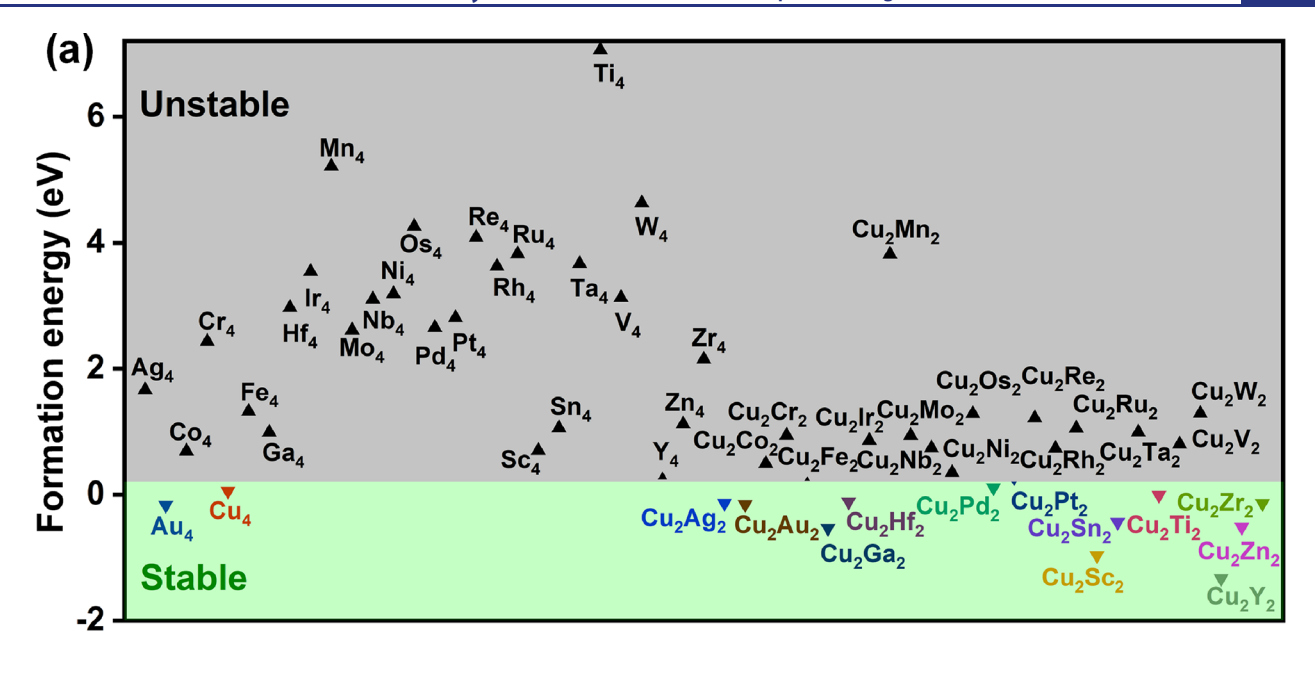
$$\Delta E_{\rm a}(^{*}CO) = E(^{*}CO) - E_{\rm sub} - E(CO)$$
(3)

$$\Delta E_{\rm a}(^*{\rm H}) = E(^*{\rm H}) - E_{\rm sub} - \frac{1}{2} \times E({\rm H}_2)$$
 (4)

where $E(C^*O)$ and $E(H^*)$ are the total energy of the CO molecule and the H atom adsorbed on the substrate and E(CO) and $E(H_2)$ are the energies of the CO and H_2 molecules in the gas phase. The Gibbs free energy (ΔG) was defined as

$$\Delta G = \Delta E - T\Delta S + \Delta ZPE + \Delta G_U + \Delta G_{pH}$$
 (5)

where ΔE is the change of the total energy of each state. The entropy corrections $(T\Delta S)$ and the zero-point energy (ΔZPE) were calculated based on vibration analysis. All free energies are at 298.15 K, and the



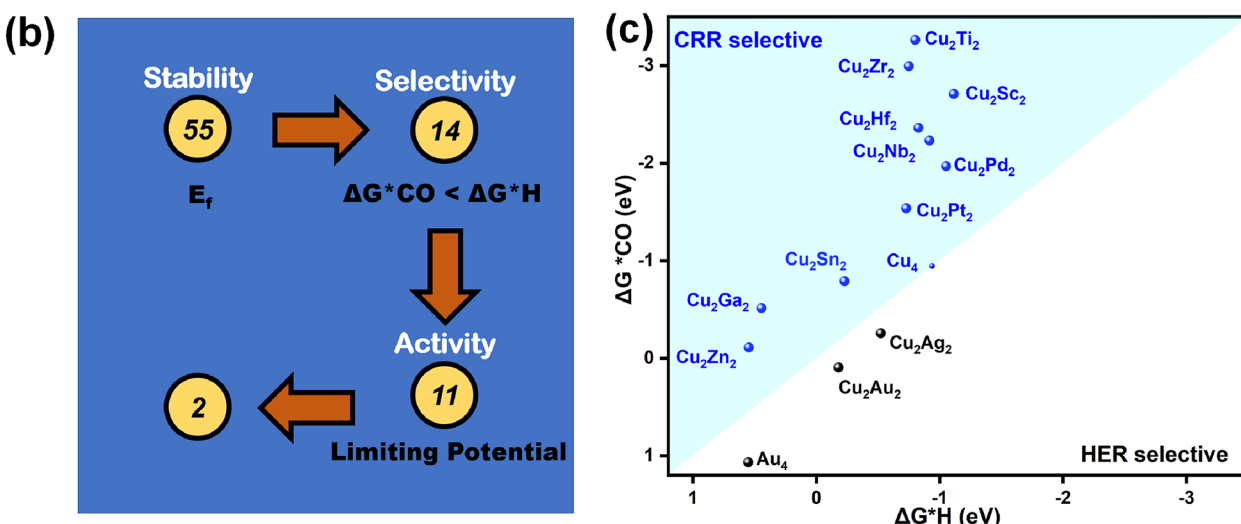


Figure 2. (a) Computed formation energies of M_4 - $C_5N_2H_2$ separated by the stability screening criterion. (b) Schematic diagram of the screening criteria for obtaining the most promising candidates. (c) The adsorption energy of the CO molecule (ΔG^*CO) compared with the hydrogen evolution reaction (ΔG^*H) based on the selectivity screening criteria.

 ΔS of CO, H₂, H₂O, C₂H₄, and CH₃CH₂OH were obtained from the NIST database. $\Delta G_{\rm U} = -neU$ is the free energy contributed by the electrode potential, where n is the number of electrons transferred, e is the amount of charge, and U is the applied potential. $\Delta G_{\rm pH} = 2.303 \times k_B T \times {\rm pH}$ represents the influence of the pH value. The computational hydrogen electrode (CHE) method was used.³⁷ The limiting potential (U_L) in full reaction path was based on

$$U_{\rm L} = -\frac{\Delta G_{\rm PDS}}{e} \tag{6}$$

where $\Delta G_{\rm PDS}$ is the free energy of the potential-determining step (PDS). The charge density difference ($\Delta \rho$) was calculated as

$$\Delta \rho = \rho(\text{sub} - \text{CO}) - \rho(\text{sub}) - \rho(\text{CO}) \tag{7}$$

where $\rho(\text{sub} - \text{CO})$ and $\rho(\text{sub})$ represent the charge density of the substrates with and without CO absorbed, respectively, and $\rho(\text{CO})$ represents the charge density of two CO molecules as absorbed.

■ RESULTS AND DISCUSSION

Structure. Conjugated macrocyclic complexes such as porphyrin structures are undoubtedly excellent catalysts for electrocatalytic reactions, and many studies on M-Pc have been reported.³⁸ Nevertheless, the pore in the middle of porphyrin can only fix one metal atom, which limits their capability to perform C₂ reduction. We innovatively replace the connecting N atom between pyrrole and pyrrole with a -C-N-Cconnection to make the pore size larger to fix more metal atoms for electrocatalytic reaction. This new structure including 8 N atoms in the pore has not been explored. The previous reports were limited to M_X - N_3 , 39 M_X - N_4 , 38,40 and M_X - N_6 . 19,22 Our proposal of M_4 - N_8 allows more active metal atoms to participate in the reaction. The bonding strength of the metal to the substrate affects the coordination environment of the metal, which in turn affects its catalytic performance. In addition, the presence of H atoms can saturate the C atoms connected to it and maintain structural stability. The structure

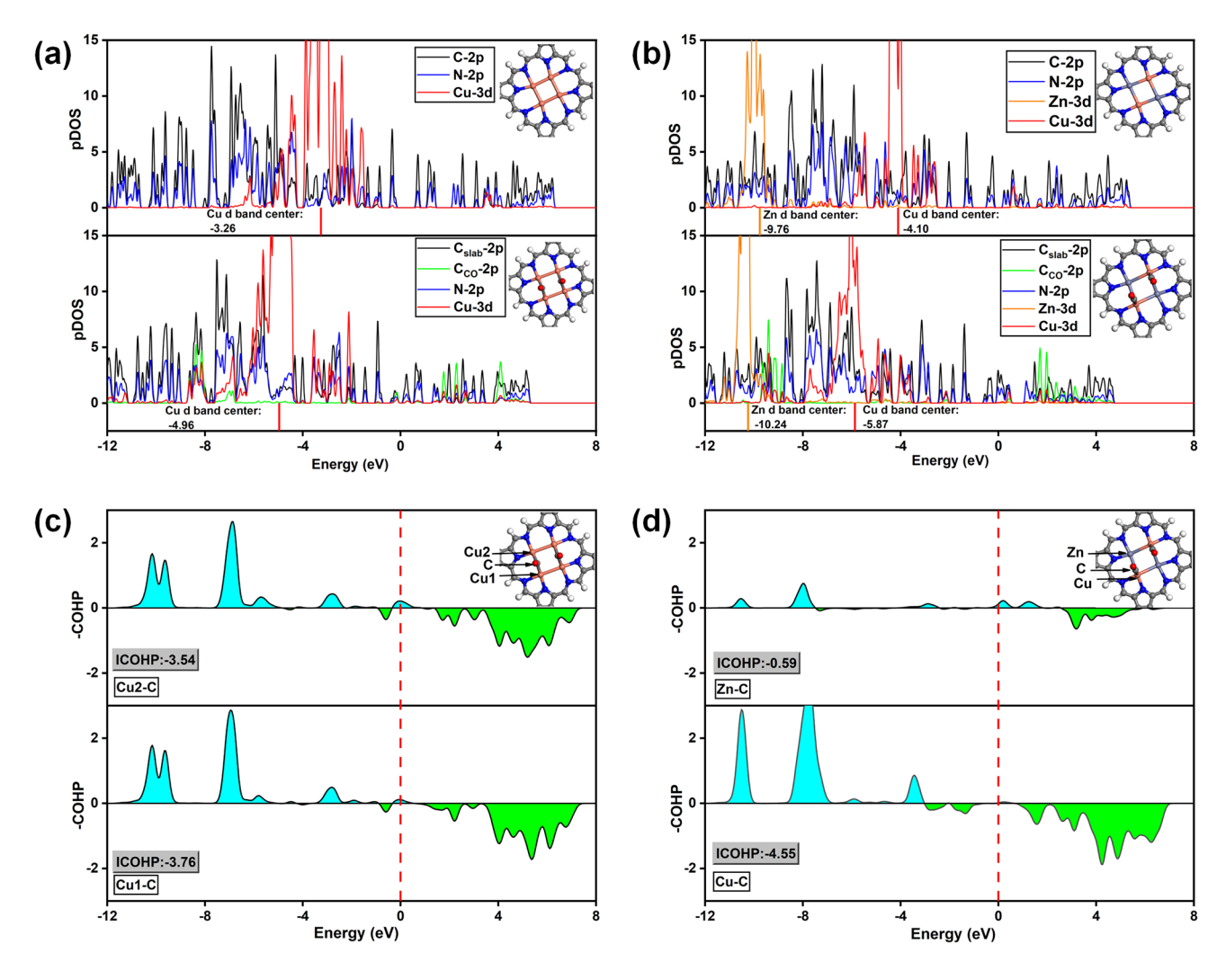


Figure 3. pDOS for (a) Cu_4 - $C_5N_2H_2$ and (b) Cu_2Zn_2 - $C_5N_2H_2$ without (top) and with (bottom) adsorbed CO molecules. The C and N atoms in the top panels are from the substate, and the C atoms in the bottom panel are either from the slab or CO, as labeled. ICOHP analysis for CO adsorption on (c) Cu_4 - $C_5N_2H_2$ and (d) Cu_2Zn_2 - $C_5N_2H_2$. E_F is set to zero. The blue and green shaded regions indicate bonding and antibonding contributions, respectively. The ICOHP value is marked in the lower left corner.

shown in Figure 1a contains 20 C atoms, 8 N atoms, and 8 H atoms in the monomer. The 8 nitrogen atoms include four pyrrole N and four linker N. The space group of the optimized monomer structure is P4/MMM, the unit cell is orthorhombic, a=b=11.81 Å, c=29.30 Å, and the pore size is 7.71 Å. Additional crystal information can be found in Table S2. A possible route to synthesize the structure is suggested in Figure S1, perhaps through two -CN or $-CH_2NH_2$ groups in a suitable chemical environment to get the key -C-N-C- linkage. 41

Dynamic Stabilities. The thermodynamic stability of $C_5N_2H_2$ was verified by AIMD calculations at 300, 500, 800, and 1000 K for 10 ps with a time step of 1 fs. Figure S2 shows the top and side views of the geometry at the end of the 10 ps. The structure at 300 K has hardly changed, and up to 1000 K, the structure remains stable. In addition, we performed the phonon spectrum calculation, as shown in Figure S3. The absence of imaginary frequencies means that the structure is dynamically stable. Furthermore, the cohesive energy of $C_5N_2H_2$ is -4.90 eV/atom, calculated by formula 1. All these facts demonstrate that $C_5N_2H_2$ is a strongly bonded network with sound stability.

Electronic Properties. The electronic properties of C₅N₂H₂ are a crucial aspect affecting its catalytic performance. We have fully investigated the band structure and partial density of states (pDOS) of C₅N₂H₂ by the HSE06 method, as shown in Figure 1b. We found that the maximum of the valence band and the minimum of the conduction band are located at the Γ point. The direct band gap is only 0.16 eV. The pDOS calculations show that both C and N atoms contribute to the conductivity. The presence of a lone pair of electrons in -C-N-C- in pyrrole to form a giant electron ring is the reason for the enhanced conductivity. In addition, we calculated the electron localization function (ELF).⁴² The ELF map ranges from 0 to 1. The region close to 1 represents strongly covalent electrons, the region close to 0 represents the region with low electron density, and the region close to 0.5 is the area of the uniform electron gas. The ELF value of the atom-to-atom connection indicates that all atoms are connected by covalent bonds (Figure S4). Both N and C atoms have sp² hybridization. The charge transfer is quantitatively characterized by the Bader charge analysis (Table S3). The two C atoms adjacent to the pyrrole N and the two C atoms around the linker N lose electrons with an

average of 0.55e and 0.54e, while the pyrrole N and the linker N gain electrons with an average of 1.05e and 1.18e. This is also demonstrated in the ELF by the high electron density in N. The electron transfer is small for the other C atoms and H atoms outside the ring. The charge transfer across this huge 24-atom ring enhances the catalytic performance, and similarly, the abundance of electrons on the N atom provides ample possibilities for metal loading and subsequent CORR.

First Screening Step: Stability. Four-atom clusters are supported on the carbon nitride framework, and it is significant to test the stability of the clusters. Taking Cu as an example, we have fully explored the adsorption of one to six Cu metal atoms in $C_5N_2H_2$ (Figure S5). The results show that the eight N atoms in the pore can be evenly distributed to coordinate the four Cu atoms, and a Cu atom connected to its surrounding two N atoms is the most stable structure. The four-atom Cu system has the lowest formation energy of 0.05 eV. Thus, Cu₄ is the most stable system among the six candidates. Further, we calculated the transition state migration barriers for Cu₄-C₅N₂H₂ to form Cu₃-C₅N₂H₂ and Cu₅-C₅N₂H₂. As shown in Figure S6, the huge energy barrier (3.98 eV) shows that the migration of a Cu atom is extremely difficult, which proves that Cu₄-C₅N₂H₂ is stable and that it is not easy for a Cu atom to migrate to form Cu₃-C₅N₂H₂ and Cu₅-C₅N₂H₂. We explored 28 homonuclear atom catalysts and 27 heteronuclear atom catalysts. As shown in Figure 2a, three screening criteria were applied to screen high-performance catalysts for CORR. The interaction between the metal and the substrate serves as the first-tier criterion for the screening of catalysts. We used the formation energy to evaluate the thermodynamic stability of the structure. By definition of formula 2, we set a criterion that $E_f < 0.2$ eV for judging the stability of a candidate. 43,44 By screening 28 systems of homonuclear metal clusters, Figure 2a, we obtained two candidates with high thermodynamic stability, namely, the Cu_4 - $C_5N_2H_2$ and Au_4 - $C_5N_2H_2$ systems.

Cu becomes our first choice as a significant metal in CO_2 reduction. Moreover, the Cu_4 - $C_5N_2H_2$ cluster is one of the few systems with a high thermodynamic stability and a negative formation energy, Figure 2a. Other 27 metals were selected to replace two of the diagonal Cu atoms in Cu_4 - $C_5N_2H_2$ to keep the overall system centrally symmetric.

Therefore, we obtained 27 Cu-based heteronuclear catalysts and also carried out the formation energy screening according to the screening criterion ($E_f \leq 0.2$), resulting in 12 stable heteronuclear systems, Cu₂Ag₂-C₅N₂H₂, Cu₂Au₂-C₅N₂H₂, Cu₂Hf₂-C₅N₂H₂, Cu₂Pd₂-C₅N₂H₂, Cu₂Pt₂-C₅N₂H₂, Cu₂Sc₂-C₅N₂H₂, Cu₂Sn₂-C₅N₂H₂, Cu₂Ti₂-C₅N₂H₂, Cu₂Y₂-C₅N₂H₂, Cu₂Zn₂-C₅N₂H₂, and Cu₂Zr₂-C₅N₂H₂.

Here, we considered the possibility of heteronuclear AABB type catalysts, as shown in Figure S7. Among the 12 heteronuclear catalysts screened by formation energy, the formation energy of the diagonal-ABAB arrangement is always lower than that of the ortho-arrangement, and the diagonal catalyst is more stable than the ortho catalyst. Since each Cu atom in the diagonal position connects to two other metal atoms at the same time, the regulation of the catalytic center can be more effective. Therefore, we consider diagonal ABAB catalysts rather than AABB catalysts.

We also studied the thermodynamic stability of Cu_4 - $C_5N_2H_2$ and Cu_2Zn_2 - $C_5N_2H_2$ through AIMD at 300, 500, 800, and 1000 K for 10 ps with a 1 fs time step. As shown in Figures S8 and S9, the temperature and energy are oscillating regularly

near the average value, demonstrating that the Cu_4 and Cu_2Zn_2 clusters are stably embedded into the $C_5N_2H_2$ framework.

Second Screening Step: Selectivity. Gas adsorption is crucial to the reaction, affecting the selectivity of the reaction in which there are two competitive pathways: CORR and hydrogen evolution reaction (HER). As shown in Figure 2c, the Faraday efficiency for the CO reduction process will be suppressed by the competing HER if the adsorption energy for HER is more negative than that of CO. If the adsorption energy of CO is more negative than that for HER, then CO reduction reaction is favored over HER. We screened 14 candidates based on CORR vs HER selectivity, Au_4 - $C_5N_2H_2$, Cu_2Ag_2 - $C_5N_2H_2$, and Cu_2Au_2 - $C_5N_2H_2$ are excluded since HER is favored, and the other 11 candidates are left for the next screening step, since CORR is favored.

Electronic Properties of M₄-C₅N₂H₂. As shown in Figure 3a, we calculated pDOS of Cu_4 -C₅N₂H₂ and Cu_2Zn_2 -C₅N₂H₂. In the Cu_4 -C₅N₂H₂ system, the 3d orbital of Cu overlaps with the 2p orbital of C and the 2p orbital of N. The N atom undergoes sp² hybridization and exchanges electrons with the 3d orbital of Cu forming a bond, which is also the reason why the metal is supported on the substrate. In comparison, in Cu_2Zn_2 -C₅N₂H₂, there is no Zn peak around the Fermi level since Zn has a 3d orbital full of electrons. Through Bader charge analysis (Table S3), we observe that Cu loses an average of 0.34 e in Cu_4 -C₅N₂H₂ if compared with free Cu atoms. In Cu_2Zn_2 -C₅N₂H₂, Zn loses an average of 0.73 e and Cu loses an average of 0.43 e if compared with free atoms.

CO Adsorption. The $C_5N_2H_2$ structure has eight N atomic sites and an inner pore of about 7.7 Å for the immobilization of metal atoms. As shown in Figure S10, we counted the distances of the four pairs of diagonal N atoms of the 11 candidates before and after CO adsorption. Taking C₅N₂H₂ as an example, the distances between the N atoms in the diagonal connection -C-N-C- are 7.7 Å, line 1 and line 3. The diagonal distances of the pyrrole N atoms are 7.4 Å, line 2 and line 4. When the metal is embedded into $C_5N_2H_2$, the four pairs of the distances of the 11 candidates change to varying degrees, which means that C5N2H2 has a certain flexibility, and its pore size can fluctuate to some extent. The maximum fluctuation is Cu_2Y_2 - $C_5N_2H_2$, line 1 = 9.3 Å, line 3 = 6.3 Å, while line 2 and line 4 are 7.6 Å. We found that the distance change of line 1 and line 3 is significantly higher than that of line 2 and line 4 after metal cluster embedding. We hypothesize that this is because the -C-N-C- linker is more flexible than pyrrole. Notably, due to the abundant fourmetal active sites, there is sufficient space and activity to simultaneously adsorb two CO molecules. Taking Cu₄-C₅N₂H₂ as an example, Figure S11, we tested three possible adsorption configurations through geometric optimization. The first scheme is that two CO molecules are adsorbed on two adjacent Cu atoms. The second scheme is that both CO molecules are adsorbed on the bridge position of two Cu atoms. The third scheme is that two CO are adsorbed on two diagonal Cu atoms. The adsorption environments of CO in the three adsorption patterns are all symmetrical. Among the three adsorption modes, the first and third schemes both use only two Cu atoms and ignore the effect of the other two Cu metal atoms. The second bridge-bridge adsorption makes full use of four Cu atoms and is the most stable configuration for the Cu₄-C₅N₂H₂ system. The CO co-adsorption energy is used as an important index to evaluate the CO capture ability of the substrate. As shown in Figure S12, compared with the

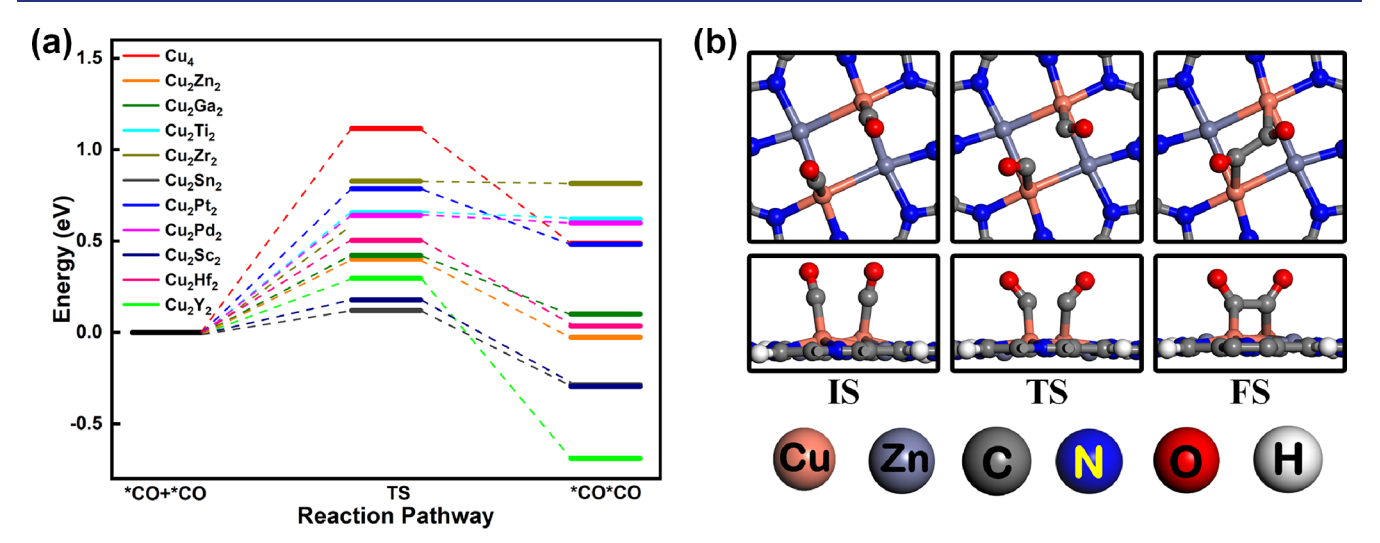


Figure 4. IS, TS, and FS energy changes involved in the reaction *CO + *CO *CO for the 11 candidates (a) and structure diagrams (b) of top view and side view for $Cu_2Zn_2-C_5N_2H_2$.

homonuclear Cu system, the introduction of Y, Zn, and Sn significantly weakens the influence of the substrate on CO, while the introduction of Ga, Pt, Sc, Pd, Hf, Zr, and Ti further increases the adsorption energy. Taking $Cu_4\text{-}C_5N_2H_2$ and $Cu_2Zn_2\text{-}C_5N_2H_2$ as examples, the co-adsorption energies of the two CO molecules are calculated to be -0.94 and -0.16 eV, respectively. The C–O bond length in $Cu_4\text{-}C_5N_2H_2$ is extended from 1.14 Å for isolated CO to 1.20 Å in the adsorbed state. This is attributed to the bonding of C atoms with two Cu atoms on the substrate with the C–Cu bond length of 1.89 Å. The C–Cu bonding weakens the interaction between the C and O atoms. The C–O bond length in $Cu_2Zn_2\text{-}C_5N_2H_2$ is 1.16 Å, a bit longer than 1.14 Å in free CO, which means that the adsorption of CO on the Cu_2Zn_2 system is weak.

The same situation is viewed in charge density difference. It can be clearly seen from Figure S13 that the interaction between Cu₄-C₅N₂H₂ and CO is stronger than between Cu₂Zn₂-C₅N₂H₂ and CO. The charge is increased on the CO molecule, and the charge-deficient area is between the two CO molecules, while in Cu₂Zn₂-C₅N₂H₂, the interaction between Zn atoms and CO is weak. In this regard, we performed pDOS and integrated-crystal orbital Hamilton population (ICOHP) analyses on the two candidates. The upper and lower panels of Figure 3a show pDOS of the substrate and CO adsorbed on the substrate, respectively. It can be concluded that the orbital overlap between the C atom and the N atom in the substrate promotes the transfer of electrons in C₅N₂H₂. In addition, it can be seen that in the process of CO adsorption, the 3d orbital of Cu and the 2p orbital of C in CO hybridize, which weakens bonding in CO and completes the adsorption process. Furthermore, due to the adsorption of CO, the d-band center of Cu is farther away from the Fermi level. In comparison in Figure 3b, the involvement of the Zn atom greatly reduces the CO adsorption. The 3d orbitals of Zn are completely occupied in Cu₂Zn₂-C₅N₂H₂, so that Zn will not undergo significant electron transfer activities with CO. Similarly, comparing the upper panels of Figure 3a and Figure 3b, the introduction of Zn causes the d-band center of Cu to move away from the Fermi level, which weakens the adsorption of CO. The results of ICOHP also confirm this conclusion. The more negative ICOHP, the stronger the adsorption. We tested the bonding effect with the C atom in CO and the two metal atoms connected to it, the ICOHP of the two Cu and C atoms in $Cu_4\text{-}C_5N_2H_2$ are -3.76 and -3.54, respectively. These values are not much different, and the bonding effect is significant. In $Cu_2Zn_2\text{-}C_5N_2H_2$, the ICOHPs between the Cu or Zn and C atoms are -4.55 and -0.59, respectively. Compared with the homonuclear system, the effect of Cu is further amplified in the Cu_2Zn_2 system, while the interaction between Zn and C is weaker.

The ICOHPs between metal atoms and between metal and substrate N atoms also change in Cu₄-C₅N₂H₂ and Cu₂Zn₂-C₅N₂H₂ before and after CO adsorption, as shown in Figure S14. Take the Cu1 atom in the Cu_4 - $C_5N_2H_2$ as an example. We investigated the bonding of Cu1 to the nearest (N1 and N2) and next closest (N3 and N8) substrate N atoms. The bond between Cu1 and the next nearest N atom (Cu1-N3 and Cu1-N8) is very weak, and the bond between Cu1 and the nearest N atom is significant. The bond between C1 and the pyrrole N atom (Cu1-N1) is stronger than that between Cu1 and the linker N atom (Cu1-N2). The same conclusion can also be obtained for the Zn atom in Cu₂Zn₂-C₅N₂H₂; moreover, the bond of Zn and substrate N atoms is stronger than Cu and substrate N atoms. As shown in Figure S14a, except for the slight weakening of the bonding strength of Cu2-N3 and Cu4-N7 after adsorption, the bonding strength of Cu and the substrate N atoms is mostly enhanced, and the bonding between Cu and Cu atoms is weakened, which means that the Cu cluster has split from the cluster into monoatomic trends after the CO adsorption. In addition, we found that after adsorption, the pore size of line 1 to line 4 increased slightly (average ~ 0.1 Å), which also confirms the conclusion above. In Cu₂Zn₂-C₅N₂H₂, Figure S14b, there is little difference in the bonding between the metal and the substrate N atoms after the adsorption. The bonding between adjacent metal atoms is generally weakened.

C–C Coupling. Following the CO adsorption, successful coupling of two C atoms is a vital step for CO to generate C₂ products. Our designed structure both provides sufficient active sites for simultaneous adsorption of two CO molecules, and positions the CO molecules close to each other. Thus, the system is fully prepared for the subsequent coupling. We performed C–C coupling transition state calculations for the

eight systems mentioned above. As shown in Figure 4, the reaction energy barrier of Cu₄-C₅N₂H₂ is about 1.12 eV. The introduction of heteronuclear metals further lowers the transition state energy barrier. Taking Cu₂Zn₂-C₅N₂H₂ as an example, the energy barrier of the transition state is 0.40 eV, which means that Cu₂Zn₂-C₅N₂H₂ is more prone to *CO + *CO \rightarrow *CO*CO than Cu₄-C₅N₂H₂. The distance between the two C atoms also changes from 3.31 to 2.29 Å in the transition state, and in the final state structure, the distance is 1.55 Å, which marks the end of this step of the reaction.

Full Path Calculations. Regarding the formation of the C₂ products, we considered ethylene or ethanol as the final product and calculated the energies of the intermediates in each step. We calculated the whole pathways of 11 candidates. The reaction paths of nine of these catalysts can be viewed in Figure S15. Cu₄-C₅N₂H₂ and Cu₂Zn₂-C₅N₂H₂ catalyze CO to the C_2 product, the reactions are as follows:

$$2CO + 8H^{+} + 8e^{-} \rightarrow C_{2}H_{4} + 2H_{2}O$$
 (8)

$$2CO + 8H^{+} + 8e^{-} \rightarrow C_{2}H_{5}OH + H_{2}O$$
 (9)

Both reactions are 8-electron processes. As shown in Figures 5 and 6, we have fully explained the significant role of C-C coupling in the whole reaction. The subsequent four-step H addition process of *CO*CO in the Cu₄-C₅N₂H₂ system is exothermic phenomenon (O*C*CO + H⁺ → *COH*CO, *COH*CO+ H+ \rightarrow *COH*COH, *COH*COH + H+ \rightarrow *C*COH + H_2O , *C*COH + $H^+ \rightarrow$ *CH*COH), which means that the entire reaction will proceed spontaneously

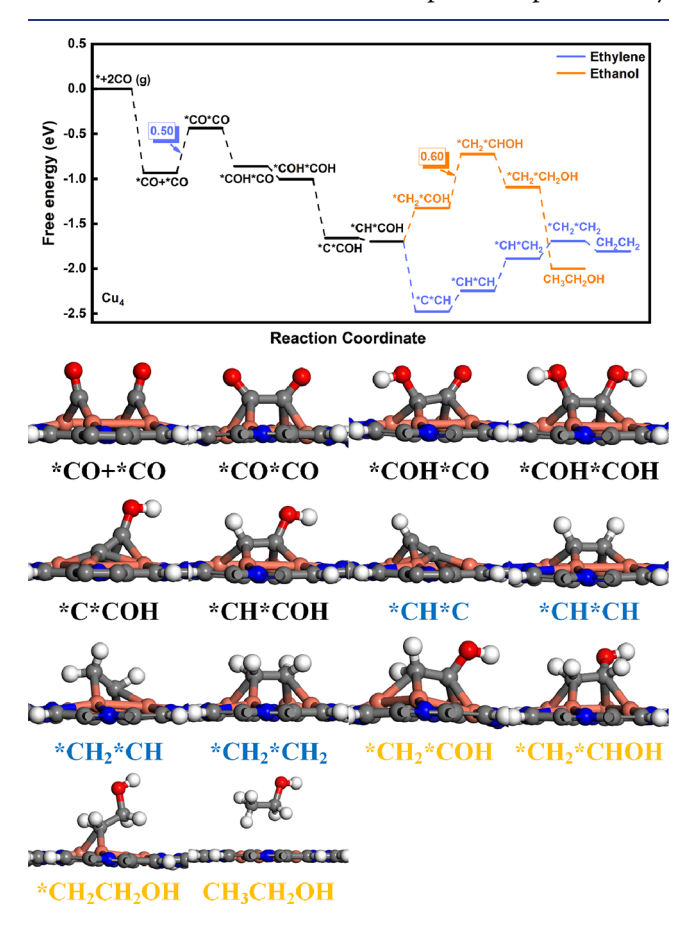


Figure 5. Free energy diagram and optimized structures of the CORR pathways to CH₂CH₂ and CH₃CH₂OH on Cu₄-C₅N₂H₂.

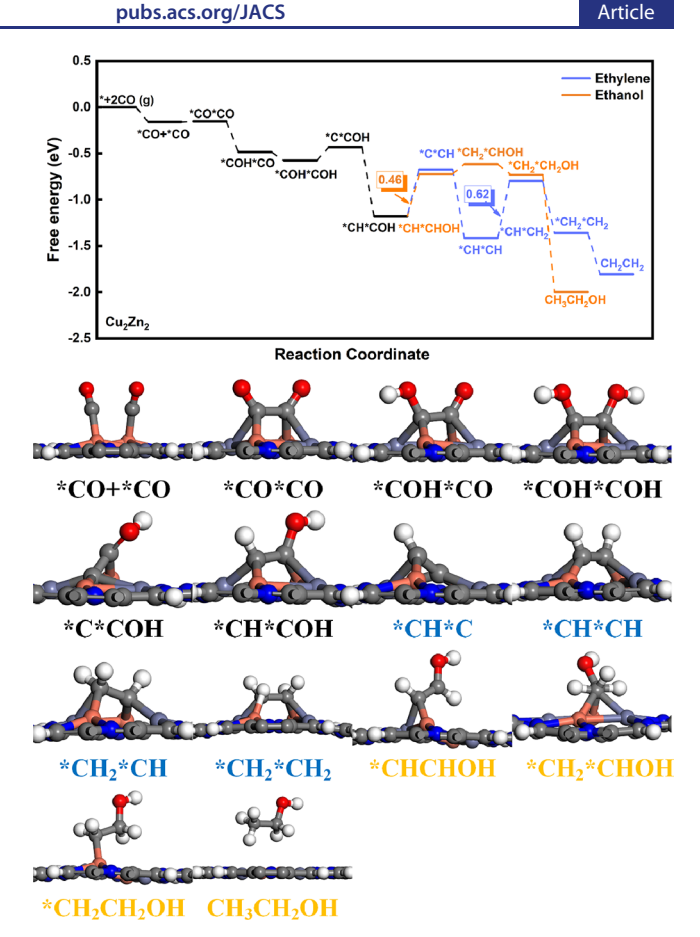


Figure 6. Free energy diagram and optimized structures of the CORR pathways to CH₂CH₂ and CH₃CH₂OH on Cu₂Zn₂-C₅N₂H₂.

without the need for an applied voltage. We previously demonstrated that the intermediate *CH*COH is the key step in determining whether the product is ethanol or ethylene in this process.¹⁹ If the ethylene path is followed, *CH*COH + $H^+ \rightarrow *CH*C + H_2O$ will occur. If the system follows the ethanol route, there will be two possibilities due to the difference of the H site, namely, $*CH*COH + H^+ \rightarrow$ *CH*CHOH and *CH*COH + $H^+ \rightarrow *CH_2*COH$. The same situation occurs in the protonation process of *CH₂*CHOH. It is also worth discussing whether it is $*CH_2*CHOH+H^+ \rightarrow *CH_3*CHOH \text{ or } *CH_2*CHOH+H^+$ \rightarrow *CH₂*CH₂OH.

Taking Cu₄-C₅N₂H₂ as an example (Figure 5), the protonation of *CH*COH is more inclined to generate *CH*C (-0.78 eV), and the potential-determining step of generating ethylene is the step of $*CO + *CO \rightarrow *CO*CO$, which is only 0.50 eV. In the route of generating ethanol, the potential-determining step is *CH2*COH + H⁺ → *CH₂*CHOH (0.60 eV), which means that Cu₄-C₅N₂H₂ has excellent selectivity for ethylene. Therefore, ethylene is expected in the product. As shown in Table S4, we counted some of the reported PDS in CORR or CO2RR and their corresponding $U_{\rm L}$. Our work provides a relatively low energy barrier strategy for the generation of ethylene with C_{2+} as the target product.

As for Cu_2Zn_2 - $C_5N_2H_2$ (Figure 6), *CH*COH + H⁺ \rightarrow *CH*CHOH is the reaction with the lowest energy and the highest possibility, and this step is the potential-determining step on the route to ethanol, which is only 0.46 eV. The subsequent protonation process of *CH*CHOH does not rule

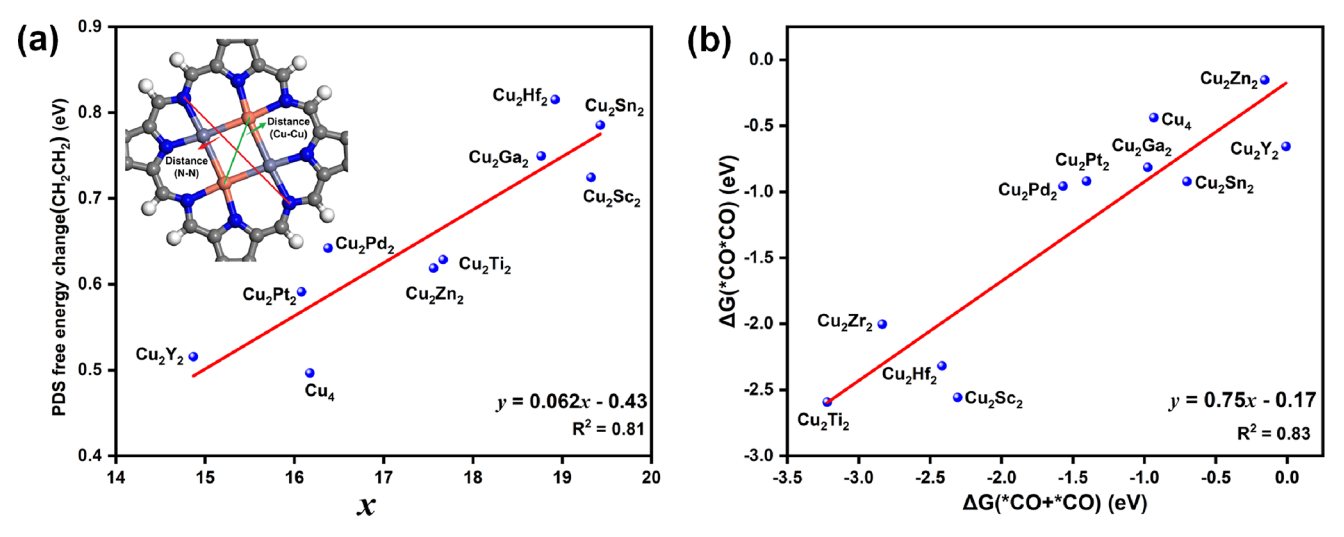


Figure 7. (a) descriptor (x) versus the potential determining step free energy change of ethylene generation in CORR. (b) Adsorption energy of two CO molecules before ($\Delta G(*CO + *CO)$) and after ($\Delta G(*CO*CO)$) C-C coupling.

out dehydration of the hydroxyl group. Similarly, we can find that in the same electronic reaction process, the energy of the alkene-generating pathway is lower than that of the ethanolgenerating pathway. For example, the subsequent formation of *CH*CH from *CH*CHOH is significantly more likely than that of *CH2*CHOH, and *CH2*CH is also easier to obtain than CH₂CH₂OH. The potential-determining step for the formation of ethylene is $*CH*CH + H^+ \rightarrow *CH_2*CH$, which is 0.62 eV. In addition, we consider the effect of pH in Cu₄-C₅N₂H₂ and Cu₂Zn₂-C₅N₂H₂, Figures S16 and S17. We have considered the cases of pH = 0, 1, 7 and 13. The energy barrier of the potential determining step increases with the increase of pH, while the potential-determining-step itself does not change.

Universal Descriptor of Catalytic Performance. To better understand the catalytic performance exhibited by the catalysts, we performed Least Absolute Shrinkage and Selection Operator (LASSO)⁴⁶ analysis to find a novel descriptor, the LASSO regression generates a huge date set and then filters out the descriptors with the best linear relationship. We entered the number of valence electrons in the d orbital (N_d) , electronegativity (E_{σ}) , and atomic radius (R) of the metal atom as input variables in LASSO. In addition, we also collected structural parameters as input variables, including $D_{(Cu-Cu)}$, which is the distance between diagonal Cu metals, and $D_{(N-N)} - 2 \times R_N$ (where $D_{(N-N)}$ is the distance between diagonal nitrogen atoms, R_N , is the radius of N atoms), and ICOHP based on metal atoms and C atoms in adsorbed CO. After LASSO regression, we obtained an integrated descriptor as following:

$$x = D_{(Cu-Cu)} \times (D_{(N-N)} - 2 \times R_N)$$
(10)

We use $D_{(N-N)} - 2 * R_N$ as the input variable, in order to express the actual vacuum distance between the two N atoms.

It can be seen from Figure 7a that the descriptor we discover has a great linear relationship with potential determining step (PDS) free energy change of ethylene, $R^2 = 0.81$. When different metal atoms are introduced, the M₄-C₅N₂H₂ skeleton has a certain flexibility, resulting in a certain degree of change in the distance between the two diagonally positioned Cu atoms and the diagonally positioned N atoms. When $D_{(Cu-Cu)}$ and $D_{(N-N)}$ are smaller, and the descriptor (x) is smaller, the potential-determining step for CORR to ethylene is also smaller, so that the candidate has extremely high catalytic activity, and the introduction of atoms leads to changes in some characteristic values of the material. Thus, establishing a connection between the flexibility and the potential-determining step energy barrier is the highlight, and to our knowledge, no relevant reports have appeared before this.

In addition, as shown in Figure 7b, we find that there is a good linear relationship between the adsorption energy before and after the C-C coupling, $R^2 = 0.83$, which means that the adsorption energy in the *CO + *CO state corelates to the corresponding energy in the *CO*CO state. It is worth mentioning that the difference between y and x, which means the energy difference of the C–C coupling step, z = y - x = -0.25x - 0.17, can be used to represent the energy difference of C–C coupling. We found that when x is more positive and z is more negative, the C-C coupling is easier.

Grand Canonical DFT Calculations for Cu₄-C₅N₂H₂. The traditional density functional theory usually assumes that the catalyst has a constant number of electrons. Such calculation is called the charge-neutral method (cnm). However, in the electrochemical system, extensive electron transfer occurs between the catalyst and electrode to complete the reaction, and the potential is constant. This corresponds to the constant potential model (cpm). The grand canonical DFT (GC-DFT) calculations are considered as a powerful theory to model the actual electrochemical system.⁴

As shown in Figure S18, we calculated the whole process of CO reduction to C₂H₄ in Cu₄-C₅N₂H₂. It can be found that the PDS in cnm is the same as that in cpm, and both are *CO + *CO → OCCO, with the energy change in the cnm being 0.50 eV and 0.59 eV for cpm. During the reaction process, the trend of energy change is similar between cnm and cpm. In addition, as shown in Figure S19, we simulated the possibility of C-C coupling of Cu₄-C₅N₂H₂ at different applied potentials by the cpm method. We changed the applied potential from 0 to -0.5 V and found that the more negative the applied potential, the lower the energy barrier between the transition state (TS) and the initial state (IS), and the easier the reaction to occur. This is consistent with the actual electrochemical reaction.

CONCLUSIONS

In summary, we have designed a 2D carbon nitride material with a centrosymmetric N8 site, as a new type of narrow-gap semiconductor ($E_g = 0.16 \text{ eV}$) with sound electrical conductivity and stability. After screening 28 homonuclear and 27 heteronuclear catalysts and analyzing the catalytic performance of the candidates, we have identified Cu₄-C₅N₂H₂ and Cu₂Zn₂-C₅N₂H₂ as the best systems for CO reduction. Cu₄-C₅N₂H₂ has high activity for producing ethylene. The energy barrier of the potential-determining step is 0.50 V. Cu₂Zn₂-C₅N₂H₂ is an excellent catalyst for ethanol synthesis. The corresponding potential-limiting step is even lower, only 0.46 V. Through LASSO regression, we have demonstrated the flexibility-related descriptor $D_{(Cu-Cu)} \times (D_{(N-N)} - 2 \times R_N)$ that relates the properties of the substrate, the supported metal, and $U_{\rm L}$. The four-atom catalysis strategy demonstrated in our study provides more options for tuning the catalytic performance, compared with single-atom catalysis, since it allows for more active sites and pathways for CORR. The strategy offers a novel scheme for exploring polyatomic catalytic CO reduction reactions.

ASSOCIATED CONTENT

Supporting Information

The Supporting Information is available free of charge at https://pubs.acs.org/doi/10.1021/jacs.3c01561.

Thermodynamic data, structural information, synthesis path, ab initio MD data, phonon spectrum, electron localization function, Bader charge, formation, pore size, adsorption patterns, adsorption energies, charge density difference, energy barrier diagrams, crystal orbital Hamilton population analyses, comparison with other catalysts (PDF)

AUTHOR INFORMATION

Corresponding Authors

Oleg V. Prezhdo – Department of Chemistry, University of Southern California, Los Angeles, California 90089, United States; Oorcid.org/0000-0002-5140-7500;

Email: prezhdo@usc.edu

Lai Xu — Jiangsu Key Laboratory of Advanced Negative
Carbon Technologies, Jiangsu Key Laboratory for CarbonBased Functional Materials & Devices, Joint International
Research Laboratory of Carbon-Based Functional Materials
and Devices, Institute of Functional Nano & Soft Materials
(FUNSOM), Soochow University, Suzhou 215123 Jiangsu,
PR China; orcid.org/0000-0003-2473-3359;
Email: xulai15@suda.edu.cn

Linan: Adia115(03dda

Author

Dewei Zhang — Jiangsu Key Laboratory of Advanced Negative Carbon Technologies, Jiangsu Key Laboratory for Carbon-Based Functional Materials & Devices, Joint International Research Laboratory of Carbon-Based Functional Materials and Devices, Institute of Functional Nano & Soft Materials (FUNSOM), Soochow University, Suzhou 215123 Jiangsu, PR China

Complete contact information is available at: https://pubs.acs.org/10.1021/jacs.3c01561

Notes

The authors declare no competing financial interest.

ACKNOWLEDGMENTS

L.X. acknowledges financial support from the National Natural Science Foundation of China-Major Research Plan (91961120), the National Natural Science Foundation of China-General Program (22273063), and the Major Program in Jiangsu University Natural Science Research (21KJA150004). O.V.P. acknowledges support of the US National Science Foundation (CHE-2154367). This work is also supported by Suzhou Key Laboratory of Functional Nano & Soft Materials, Collaborative Innovation Center of Suzhou Nano Science & Technology, and the 111 Project.

REFERENCES

- (1) Su, Y.; Wang, Z.; Legrand, A.; Aoyama, T.; Ma, N.; Wang, W.; Otake, K. I.; Urayama, K.; Horike, S.; Kitagawa, S.; Furukawa, S.; Gu, C. Hypercrosslinked Polymer Gels as a Synthetic Hybridization Platform for Designing Versatile Molecular Separators. *J. Am. Chem. Soc.* 2022, 144, 6861–6870.
- (2) Gu, C.; Hosono, N.; Zheng, J. J.; Sato, Y.; Kusaka, S.; Sakaki, S.; Kitagawa, S. Design and Control of Gas Diffusion Process in a Nanoporous Soft Crystal. *Science* **2019**, *363*, 387–391.
- (3) Su, Y.; Li, B.; Xu, H.; Lu, C.; Wang, S.; Chen, B.; Wang, Z.; Wang, W.; Otake, K. I.; Kitagawa, S.; Huang, L.; Gu, C. Multi-Component Synthesis of a Buta-1,3-diene-Linked Covalent Organic Framework. J. Am. Chem. Soc. 2022, 144, 18218–18222.
- (4) Li, Y.; Yang, L.; He, H.; Sun, L.; Wang, H.; Fang, X.; Zhao, Y.; Zheng, D.; Qi, Y.; Li, Z.; Deng, W. In situ Photodeposition of Platinum Clusters on a Covalent Organic Framework for Photocatalytic Hydrogen Production. *Nat. Commun.* **2022**, *13*, 1355.
- (5) Su, Y.; Otake, K. I.; Zheng, J. J.; Horike, S.; Kitagawa, S.; Gu, C. Separating Water Isotopologues Using Diffusion-Regulatory Porous Materials. *Nature* **2022**, *611*, 289–294.
- (6) Zhou, W.; Deng, Q. W.; He, H. J.; Yang, L.; Liu, T. Y.; Wang, X.; Zheng, D. Y.; Dai, Z. B.; Sun, L.; Liu, C.; Wu, H.; Li, Z.; Deng, W. Q. Heterogenization of Salen Metal Molecular Catalysts in Covalent Organic Frameworks for Photocatalytic Hydrogen Evolution. *Angew. Chem., Int. Ed.* **2023**, 62, No. 202214143.
- (7) Kuhl, K. P.; Cave, E. R.; Abram, D. N.; Jaramillo, T. F. New Insights into the Electrochemical Reduction of Carbon Dioxide on Metallic Copper Surfaces. *Energy Environ. Sci.* **2012**, *5*, 7050–7059.
- (8) Nitopi, S.; Bertheussen, E.; Scott, S. B.; Liu, X. Y.; Engstfeld, A. K.; Horch, S.; Seger, B.; Stephens, I. E. L.; Chan, K.; Hahn, C.; Norskov, J. K.; Jaramillo, T. F.; Chorkendorff, I. Progress and Perspectives of Electrochemical CO₂ Reduction on Copper in Aqueous Electrolyte. *Chem. Rev.* **2019**, *119*, 7610–7672.
- (9) Qiao, J. L.; Liu, Y. Y.; Hong, F.; Zhang, J. J. A Review of Catalysts for the Electroreduction of Carbon Dioxide to Produce Low-Carbon Fuels. *Chem. Soc. Rev.* **2014**, *43*, 631–675.
- (10) Aresta, M.; Dibenedetto, A.; Angelini, A. Catalysis for the Valorization of Exhaust Carbon: from CO₂ to Chemicals, Materials, and Fuels. Technological Use of CO₂. *Chem. Rev.* **2014**, *114*, 1709–1742.
- (11) Li, C. W.; Ciston, J.; Kanan, M. W. Electroreduction of Carbon Monoxide to Liquid Fuel on Oxide-Derived Nanocrystalline Copper. *Nature* **2014**, *508*, 504–507.
- (12) Wang, L.; Nitopi, S. A.; Bertheussen, E.; Orazov, M.; Morales-Guio, C. G.; Liu, X. Y.; Higgins, D. C.; Chan, K. R.; Norskov, J. K.; Hahn, C.; Jaramillo, T. F. Electrochemical Carbon Monoxide Reduction on Polycrystalline Copper: Effects of Potential, Pressure, and pH on Selectivity toward Multicarbon and Oxygenated Products. *ACS Catal.* **2018**, *8*, 7445–7454.
- (13) Zhang, H. C.; Li, J.; Cheng, M. J.; Lu, Q. CO Electroreduction: Current Development and Understanding of Cu-Based Catalysts. *ACS Catal.* **2019**, *9*, 49–65.
- (14) Jouny, M.; Luc, W.; Jiao, F. High-Rate Electroreduction of Carbon Monoxide to Multi-Carbon Products. *Nat. Catal.* **2018**, *1*, 748–755.

- (15) Li, M. H.; Wang, H. F.; Luo, W.; Sherrell, P. C.; Chen, J.; Yang, J. P. Heterogeneous Single-Atom Catalysts for Electrochemical CO₂ Reduction Reaction. *Adv. Mater.* **2020**, 32, No. 2001848.
- (16) Chen, Y. J.; Ji, S. F.; Chen, C.; Peng, Q.; Wang, D. S.; Li, Y. D. Single-Atom Catalysts: Synthetic Strategies and Electrochemical Applications. *Joule* **2018**, *2*, 1242–1264.
- (17) Yang, X. F.; Wang, A. Q.; Qiao, B. T.; Li, J.; Liu, J. Y.; Zhang, T. Single-Atom Catalysts: A New Frontier in Heterogeneous Catalysis. *Acc. Chem. Res.* **2013**, *46*, 1740–1748.
- (18) Jiao, L.; Zhu, J.; Zhang, Y.; Yang, W.; Zhou, S.; Li, A.; Xie, C.; Zheng, X.; Zhou, W.; Yu, S. H.; Jiang, H. L. Non-Bonding Interaction of Neighboring Fe and Ni Single-Atom Pairs on MOF-Derived N-Doped Carbon for Enhanced CO₂ Electroreduction. *J. Am. Chem. Soc.* **2021**, *143*, 19417–19424.
- (19) Wang, X.; Qiu, S.; Feng, J.; Tong, Y.; Zhou, F.; Li, Q.; Song, L.; Chen, S.; Wu, K. H.; Su, P.; Ye, S.; Hou, F.; Dou, S. X.; Liu, H. K.; Max, L.; Sun, C.; Liu, J.; Liang, J. Confined Fe-Cu Clusters as Sub-Nanometer Reactors for Efficiently Regulating the Electrochemical Nitrogen Reduction Reaction. *Adv. Mater.* **2020**, *32*, No. 2004382.
- (20) Ying, Y. R.; Luo, X.; Qiao, J. L.; Huang, H. T. "More is Different:" Synergistic Effect and Structural Engineering in Double-Atom Catalysts. *Adv. Funct. Mater.* **2021**, *31*, No. 2007423.
- (21) Li, Y.; Wei, B.; Zhu, M.; Chen, J.; Jiang, Q.; Yang, B.; Hou, Y.; Lei, L.; Li, Z.; Zhang, R.; Lu, Y. Synergistic Effect of Atomically Dispersed Ni-Zn Pair Sites for Enhanced CO₂ Electroreduction. *Adv. Mater.* **2021**, 33, No. 2102212.
- (22) Zhu, J.; Xiao, M.; Ren, D.; Gao, R.; Liu, X.; Zhang, Z.; Luo, D.; Xing, W.; Su, D.; Yu, A.; Chen, Z. Quasi-Covalently Coupled Ni-Cu Atomic Pair for Synergistic Electroreduction of CO₂. *J. Am. Chem. Soc.* **2022**, *144*, 9661–9671.
- (23) Kamysbayev, V.; Filatov, A. S.; Hu, H.; Rui, X.; Lagunas, F.; Wang, D.; Klie, R. F.; Talapin, D. V. Covalent surface modifications and superconductivity of two-dimensional metal carbide MXenes. *Science* **2020**, *369*, 979–983.
- (24) Jeon, H. S.; Timoshenko, J.; Rettenmaier, C.; Herzog, A.; Yoon, A.; Chee, S. W.; Oener, S.; Hejral, U.; Haase, F. T.; Roldan Cuenya, B. Selectivity Control of Cu Nanocrystals in a Gas-Fed Flow Cell through CO₂ Pulsed Electroreduction. *J. Am. Chem. Soc.* **2021**, *143*, 7578–7587.
- (25) Gao, Z. H.; Wei, K.; Wu, T.; Dong, J.; Jiang, D. E.; Sun, S.; Wang, L. S. A Heteroleptic Gold Hydride Nanocluster for Efficient and Selective Electrocatalytic Reduction of CO₂ to CO. *J. Am. Chem. Soc.* **2022**, *144*, 5258–5262.
- (26) Prabhu, P.; Jose, V.; Lee, J. M. Heterostructured Catalysts for Electrocatalytic and Photocatalytic Carbon Dioxide Reduction. *Adv. Funct. Mater.* **2020**, *30*, No. 1910768.
- (27) Hafner, J. Ab-Initio Simulations of Materials Using VASP: Density-Functional Theory and Beyond. *J. Comput. Chem.* **2008**, 29, 2044–2078.
- (28) Perdew, J. P.; Burke, K.; Ernzerhof, M. Generalized Gradient Approximation Made Simple. *Phys. Rev. Lett.* **1996**, *77*, 3865–3868.
- (29) Blochl, P. E. Projector Augmented-Wave Method. *Phys. Rev. B* **1994**, *So.*, 17953–17979.
- (30) Grimme, S.; Antony, J.; Ehrlich, S.; Krieg, H. A Consistent and Accurate Ab Initio Parametrization of Density Functional Dispersion Correction (DFT-D) for the 94 Elements H-Pu. *J. Chem. Phys.* **2010**, 132, 154101.
- (31) Togo, A.; Oba, F.; Tanaka, I. First-Principles Calculations of the Ferroelastic Transition between Rutile-Type and CaCl₂-type SiO₂ at High Pressures. *Phys. Rev. B* **2008**, *78*, No. 134106.
- (32) Mathew, K.; Sundararaman, R.; Letchworth-Weaver, K.; Arias, T. A.; Hennig, R. G. Implicit Solvation Model for Density-Functional Study of Nanocrystal Surfaces and Reaction Pathways. *J. Chem. Phys.* **2014**, *140*, No. 084106.
- (33) Henkelman, G.; Uberuaga, B. P.; Jonsson, H. A Climbing Image Nudged Elastic Band Method for Finding Saddle Points and Minimum Energy Paths. *J. Chem. Phys.* **2000**, *113*, 9901–9904.

- (34) Heyd, J.; Scuseria, G. E.; Ernzerhof, M. Hybrid Functionals Based on a Screened Coulomb Potential. *J. Chem. Phys.* **2003**, *118*, 8207–8215.
- (35) Sundararaman, R.; Letchworth-Weaver, K.; Schwarz, K. A.; Gunceler, D.; Ozhabes, Y.; Arias, T. A. JDFTx: software for joint density-functional theory. *SoftwareX* **2017**, *6*, 278–284.
- (36) Sundararaman, R.; Goddard, W. A. The Charge-Asymmetric Nonlocally Determined Local-Electric (CANDLE) Solvation Model. *J. Chem. Phys.* **2015**, *142*, No. 064107.
- (37) Norskov, J. K.; Rossmeisl, J.; Logadottir, A.; Lindqvist, L.; Kitchin, J. R.; Bligaard, T.; Jonsson, H. Origin of the Overpotential for Oxygen Reduction at a Fuel-Cell Cathode. *J. Phys. Chem. B* **2004**, *108*, 17886–17892.
- (38) Cao, S. F.; Wei, S. X.; Wei, X. F.; Zhou, S. N.; Chen, H. Y.; Hu, Y. Y.; Wang, Z. J.; Liu, S. Y.; Guo, W. Y.; Lu, X. Q. Can N, S Cocoordination Promote Single Atom Catalyst Performance in CO₂RR? Fe-N₂S₂ Porphyrin versus Fe-N4 Porphyrin. *Small* **2021**, 17, No. 2100949.
- (39) Chen, S. X.; Li, Y. W.; Bu, Z. G.; Yang, F. Q.; Luo, J. H.; An, Q. Z.; Zeng, Z. L.; Wang, J.; Deng, S. G. Boosting CO₂-to-CO conversion on a robust single-atom copper decorated carbon catalyst by enhancing intermediate binding strength. *J. Mater. Chem. A* **2021**, *9*, 1705–1712.
- (40) Li, X.; Bi, W.; Chen, M.; Sun, Y.; Ju, H.; Yan, W.; Zhu, J.; Wu, X.; Chu, W.; Wu, C.; Xie, Y. Exclusive Ni-N₄ Sites Realize Near-Unity CO Selectivity for Electrochemical CO₂ Reduction. *J. Am. Chem. Soc.* **2017**, *139*, 14889–14892.
- (41) Xie, L. Y.; Boyle, R. W.; Dolphin, D. Porphocyanines: Expanded Aromatic Tetrapyrrolic Macrocycles. *J. Am. Chem. Soc.* **1996**, *118*, 4853–4859.
- (42) Becke, A. D.; Edgecombe, K. E. A Simple Measure of Electron Localization in Atomic and Molecular Systems. *J. Chem. Phys.* **1990**, 92, 5397–5403.
- (43) Ling, C.; Shi, L.; Ouyang, Y.; Zeng, X. C.; Wang, J. Nanosheet Supported Single-Metal Atom Bifunctional Catalyst for Overall Water Splitting. *Nano Lett.* **2017**, *17*, 5133–5139.
- (44) Xu, L.; Yang, L. M.; Ganz, E. Electrocatalytic Reduction of N_2 Using Metal-Doped Borophene. ACS Appl. Mater. Interfaces **2021**, 13, 14091–14101.
- (45) Jung, H.; Lee, S. Y.; Lee, C. W.; Cho, M. K.; Won, D. H.; Kim, C.; Oh, H. S.; Min, B. K.; Hwang, Y. J. Electrochemical Fragmentation of Cu_2O Nanoparticles Enhancing Selective C-C Coupling from CO_2 Reduction Reaction. J. Am. Chem. Soc. 2019, 141, 4624–4633.
- (46) O'Connor, N. J.; Jonayat, A. S. M.; Janik, M. J.; Senftle, T. P. Interaction Trends between Single Metal Atoms and Oxide Supports Identified with Density Functional Theory and Statistical Learning. *Nat. Catal.* **2018**, *1*, 531–539.
- (47) Sundararaman, R.; Goddard, W. A.; Arias, T. A. Grand Canonical Electronic Density-Functional Theory: Algorithms and Applications to Electrochemistry. *J. Chem. Phys.* **2017**, *146*, 114104.